The PR043 Djibouti Video: Evidence for a Hypersonic-Missile Interpretation

Devesh Nandal and Abraham Loeb
Galileo Project, Harvard University

August 6, 2026

1 Data and objective

We started with the public PR043 infrared video released by the U.S. government. The file was called `DOD_111689759.mp4`. It had a resolution of 1920×1080 pixels and a frame rate of about $29.97\,\mathrm{frames\,s^{-1}}$. The distributed file was about $11.75\,\mathrm{s}$ long. We found that the same short sequence was repeated about four times. One repeated cycle contained 88 frames and lasted about $2.94\,\mathrm{s}$.

Our main goal was to estimate the motion of the small feature that crosses the image. This required several linked steps. We first needed to locate the terrain, then stabilize the video and track the feature. We then had to convert the measured image motion into a physical velocity. That final conversion depends strongly on the unknown altitude and range of the target.

Figure 1 shows the two views used for the geolocation. The black regions in panel (a) are part of the released video and the cyan marks are sensor symbology. The small compound near the lower left and the sequence of dry-channel bends were the most useful terrain features. Panel (b) shows the same area in Google Earth with candidate ground-control points attached to the terrain.

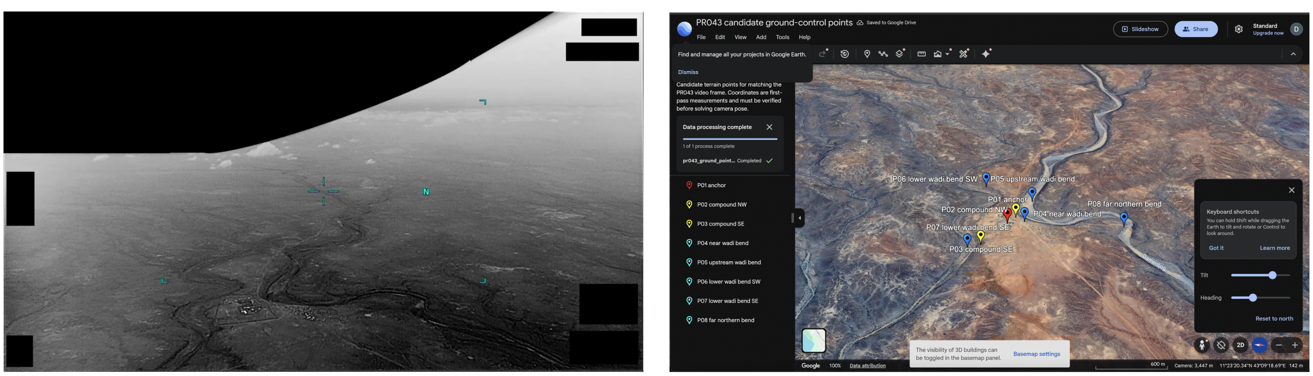

(a) Infrared reference frame.

(b) Labelled oblique Google Earth view.

Figure 1: Views used for geolocation. In panel (a), the compound lies near the lower-left wadi bend and the main channel continues toward the image centre. Panel (b) shows the matched Google Earth terrain after rotation and tilt. The compound, the nearby bend, and the more distant sequence of channel turns agree in both views. The labelled points were used as candidate terrain controls rather than as target positions.

2 Geolocation

We compared the terrain in the video with Google Maps and Google Earth. We searched for a place with the same channel bends, the same small compound, and a compatible road and ridge pattern. The best match was near

$$11.388655^\circ \text{ N}, \qquad 43.139259^\circ \text{ E}.$$

This is near Goubetto in southern Djibouti. The nearby channel belongs to the Damerjog drainage system. It resembles a river in the infrared image, but it is more likely a dry wadi or an ephemeral channel.

We produced top-down and tilted Google Earth views and placed candidate ground-control points on clear channel bends and compound features. The location match was strong because the same ordered sequence of bends and tributaries appeared in both the video and the map. The coordinate above is a ground anchor. It is not the sensor position and it is not the position of the moving target.

3 Terrain stabilization and target tracking

We next stabilized the terrain and searched for features that moved relative to the ground. The repeated video cycles were useful because they allowed us to compare the same event several times. We tracked the small contrast feature over 13 positions. The useful segment covered frames 61 to 73 of the repeated cycle, giving a measured interval of 0.4004 s.

The first track fit gave a terrain-relative image speed of about

$$806\,\text{pixels}\,\text{s}^{-1}.$$

A later full projective correction changed this only slightly to

$$801\,\text{pixels}\,\text{s}^{-1}.$$

The track was almost straight. The small deviations from a perfect line were much smaller than the total displacement.

This was the strongest direct measurement in the analysis. The released clip supports a terrain-relative image motion of about 801 pixels s^{-1}. It does not directly provide a speed in metres per second because the target range is unknown.

4 Conditional ground-plane reconstruction

We used the map coordinates and the matched image points to build a projective transformation between the video and the local terrain. This allowed us to ask a conditional question: what speed would be inferred if the changing line of sight intersected the local ground plane?

The central result was

$$3.33\,\text{km}\,\text{s}^{-1}.$$

The fitted ground-track bearing was about 65.3° true. The mapped endpoint displacement was about 1.31 km over 0.4004 s.

We quantified the sensitivity with a direct Monte Carlo perturbation test. This was not a Markov-chain Monte Carlo analysis. In each of 3000 trials, we perturbed the map points and image points within their measurement uncertainties, recalculated the projective transformation, and refitted the speed. All 3000 trials were accepted. The median was

$$3.37\,\text{km}\,\text{s}^{-1},$$

with a 68% interval of

$$2.88 - -4.02\,\text{km}\,\text{s}^{-1}$$

and a 95% interval of

$$2.52 - -4.72\,\text{km}\,\text{s}^{-1}.$$

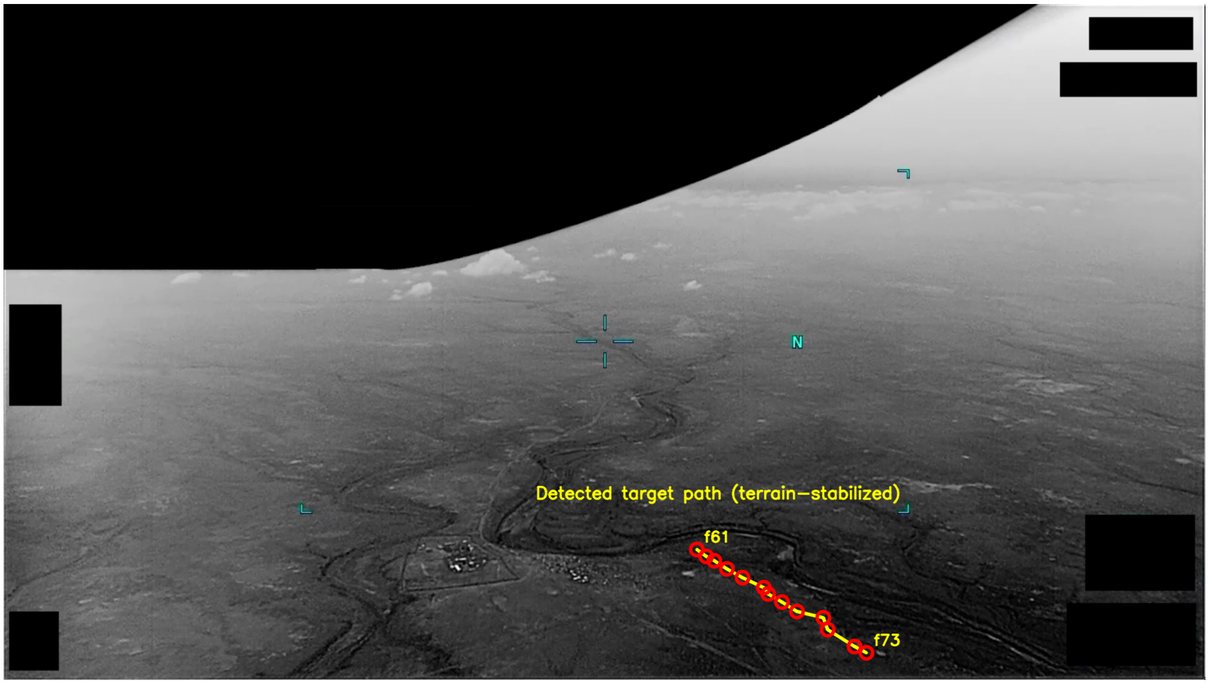

Figure 2: Terrain-stabilized target track in the full-resolution reference frame. The red circles mark the 13 measured target centroids from frame 61 to frame 73, and the yellow line shows the fitted direction of motion. The target moves toward the lower right. The small frame-to-frame departures from the line are minor compared with the total track length and are consistent with centroid and image-processing uncertainty.

This remained a ground-plane result rather than a unique target speed. The target track lay outside the convex hull of the strongest ground-control points, so the transformation was extrapolating in the target region. The result was therefore informative but not final.

5 Camera motion and differential parallax

We replaced the simpler stabilization with a full time-dependent homography that registered the terrain from frame to frame. The median registration error was about 0.228 pixels in the reduced working image, the maximum was about 0.321 pixels, and the median number of inlier terrain matches was 1736. These values showed that the background registration was stable.

The corrected target speed was

$$801.3\,\text{pixels}\,\text{s}^{-1}.$$

The largest local terrain correction was only about 0.21 full-resolution pixels. The target displacement was therefore much larger than the remaining local registration error.

We also built a conditional camera model. The internal best-fit horizontal field of view was

$$65.6^\circ,$$

with a 5% score band from 60.4° to 71.0°. Under this model, the sensor altitude was

$$\boxed{2.26\,\text{km}}$$

above the fitted local ground plane. The corresponding conditional platform speed was about $77.7\,\text{m}\,\text{s}^{-1}$. These are model-derived quantities rather than recovered aircraft telemetry.

We then tested differential parallax. A stationary object at low altitude produced only a small fraction of the observed motion. The parallax contribution increased rapidly only when the assumed target altitude approached the conditional sensor altitude.

6 Velocity and apparent size versus target altitude

We intersected each target viewing ray with a horizontal surface at a chosen altitude. This generated a family of possible physical speeds rather than one unique value. Figure 3 summarizes the result.

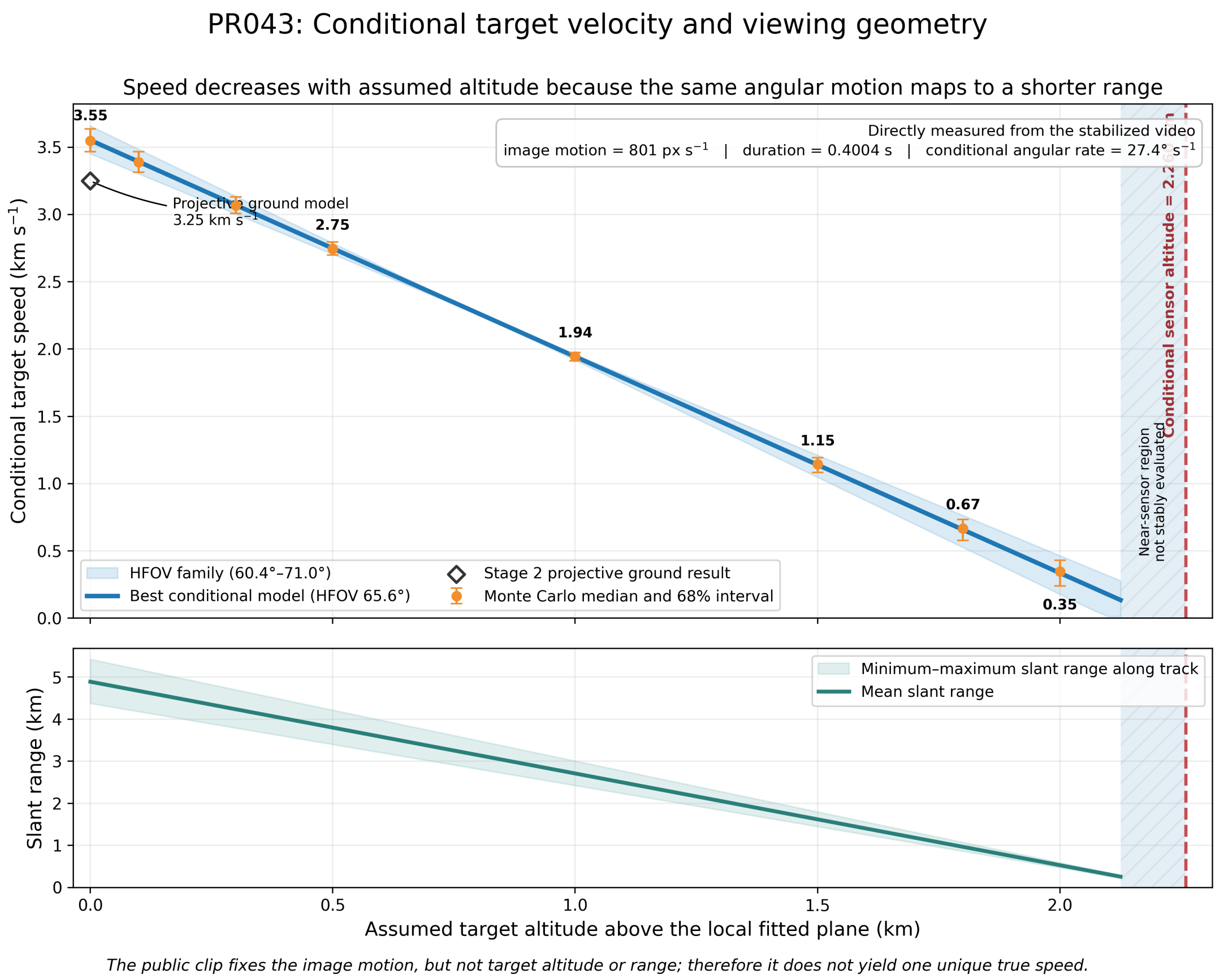

Figure 3: Conditional target velocity and viewing geometry. In the upper panel, the solid blue curve is the best conditional speed solution for an HFOV of 65.6°. The pale blue band shows the family of solutions across the accepted HFOV interval, while the orange points and error bars show the Monte Carlo median and 68% interval at selected altitudes. The open diamond is the independent Stage 2 projective ground-plane result. The red vertical dashed line marks the conditional sensor altitude, and the hatched region shows where the target approaches the sensor altitude and the reconstruction becomes unstable. The lower panel shows the corresponding mean slant range and its range along the measured track. The same angular motion maps to a shorter physical path as the assumed target altitude rises, so both inferred speed and slant range decrease.

The apparent target width was about 3.8 full-resolution pixels. Under the conditional camera model this corresponded to about 0.14°. We treated the resulting physical sizes as upper limits because the measured width includes the sensor point-spread function, compression, motion blur, registration uncertainty, and possible thermal blooming.

Table 1: Conditional target speed and apparent cross-track width at selected assumed altitudes. The width is an upper limit because the target is unresolved or only marginally resolved.

Assumed altitude	Inferred speed	Apparent width upper limit
0 m	$3.54\,\mathrm{km\,s^{-1}}$	about 12 m
500 m	$2.74\,\mathrm{km\,s^{-1}}$	about 9 m
1000 m	$1.94\,\mathrm{km\,s^{-1}}$	about 6.5 m
1500 m	$1.14\,\mathrm{km\,s^{-1}}$	about 3.9 m
1800 m	$0.66\,\mathrm{km\,s^{-1}}$	about 2.3 m
2000 m	$0.34\,\mathrm{km\,s^{-1}}$	about 1.2 m

7 Testing a missile interpretation

The velocity-altitude relation naturally raises the question of whether the moving feature could have been a missile. A numerical match to a published missile speed is not enough. A viable comparison must also satisfy the atmospheric loading, heating, drag, and acceleration implied by the same altitude. We therefore added a separate physics test based on the Stage 4 speed curve.

The Mach number was calculated from

$$M(h) = \frac{v(h)}{a(h)}, \tag{1}$$

where $a(h)$ is the local speed of sound. The dynamic pressure was

$$q(h) = \frac{1}{2}\rho(h)v(h)^2, \tag{2}$$

using a standard-atmosphere density profile. These quantities distinguish a low-altitude hypersonic solution from a high-altitude one because the same speed produces much larger aerodynamic loading in dense air.

The central curve crossed Mach 5 at an assumed target altitude of about

$$h \simeq 1.165\,\mathrm{km},$$

and the dynamic pressure fell below 1 MPa near

$$h \simeq 1.360\,\mathrm{km}.$$

At 0.5 km, the conditional solution gave Mach 8.12 and 4.407 MPa. At 1.5 km, it gave Mach 3.41 and 0.687 MPa. The low-altitude branch is therefore not only fast; it also carries severe aerodynamic loading.

We used a relative stagnation-heating proxy,

$$H_{\mathrm{rel}} = \sqrt{\frac{\rho}{\rho_{\mathrm{ref}}}}\left(\frac{v}{v_{\mathrm{ref}}}\right)^3, \tag{3}$$

Here, $v_{\mathrm{ref}} = 3.1\,\mathrm{km\,s^{-1}}$ and ρ_{ref} is the standard-atmosphere density at an altitude of 28 km. The quantity H_{rel} is therefore dimensionless and is normalized so that $H_{\mathrm{rel}} = 1$ at this reference condition. For the same nose radius and otherwise similar flow assumptions, a value of $H_{\mathrm{rel}} = 4.80$ means that the usual convective-heating scaling is 4.80 times the reference value. A value of 0.33 means that it is about one-third of the reference value. This is not a surface temperature or a heat flux in physical units. It is an order-of-magnitude heating severity indicator based on the $\sqrt{\rho}\,v^3$ scaling.

At an assumed altitude of 0.5 km, we obtained $H_{\mathrm{rel}} = 4.80$, whereas at 1.5 km we obtained $H_{\mathrm{rel}} = 0.33$. Sustained Mach-8 flight near 500 m would therefore be highly demanding. A brief terminal passage cannot be excluded because the measured track lasts only 0.4004 s.

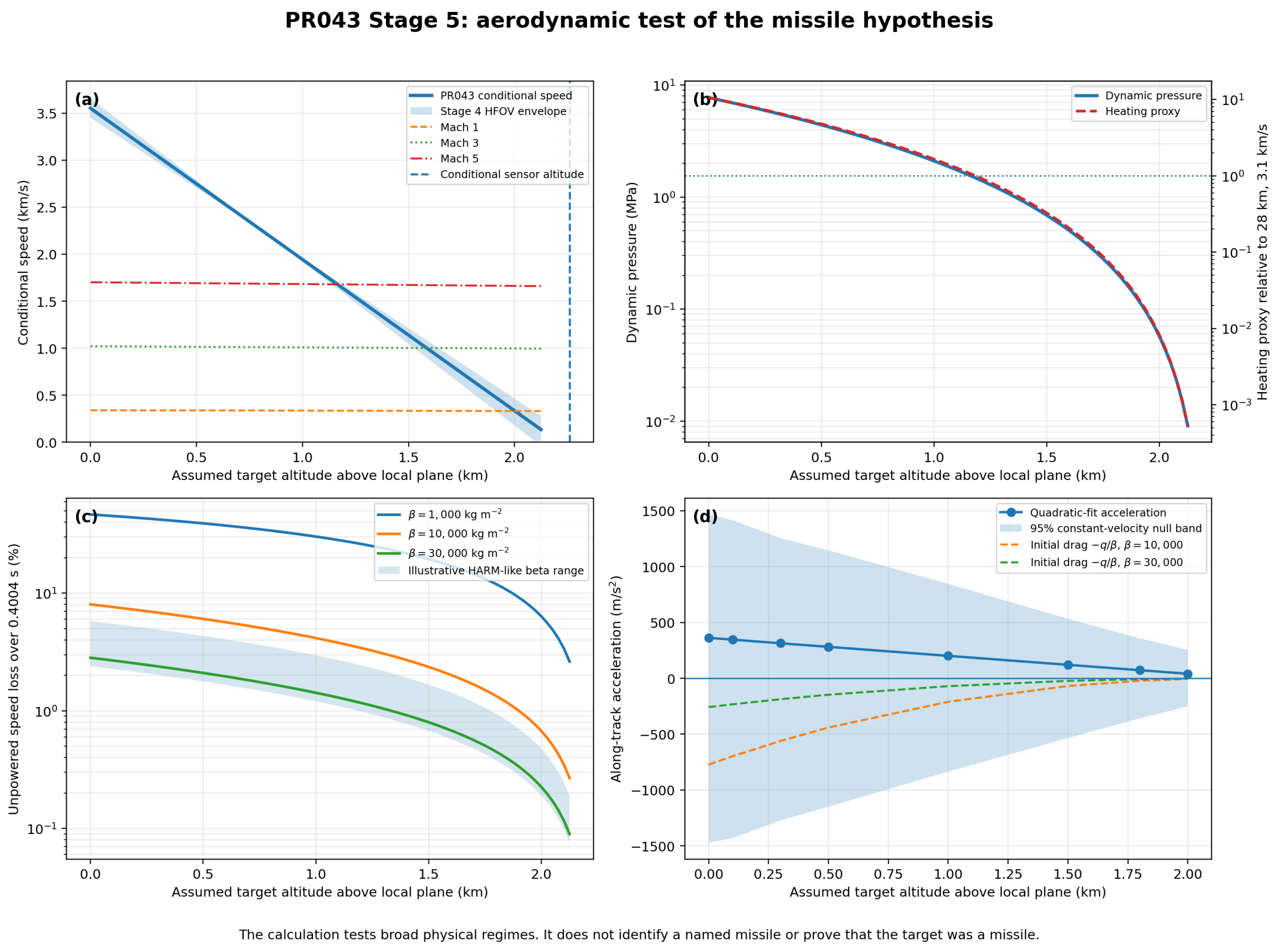

Figure 4: Aerodynamic test of the missile hypothesis. Panel (a) shows the conditional speed-altitude curve, the Mach 1, Mach 3, and Mach 5 levels, and the conditional sensor altitude. The curve is above Mach 5 below about 1.17 km. Panel (b) shows dynamic pressure and the relative heating proxy on logarithmic axes; both rise steeply toward the low-altitude branch, which is why sustained low-altitude hypersonic flight is difficult. Panel (c) shows the predicted unpowered speed loss during the observed 0.4004 s interval for several ballistic coefficients. Dense, streamlined objects with large β lose only a few percent of their speed over this short interval. The shaded strip marks the illustrative HARM-like ballistic-coefficient range. Panel (d) compares the fitted along-track acceleration with the 95% constant-velocity bootstrap band and with representative initial drag decelerations. The fitted acceleration remains well inside the null band at every selected altitude, so the track does not distinguish propulsion from high-β coasting.

7.1 Unpowered drag and ballistic coefficient

We described the object's drag response with the ballistic coefficient

$$\beta = \frac{m}{C_D A}, \tag{4}$$

where m is mass, C_D is drag coefficient, and A is reference area. The one-dimensional drag equation is

$$\frac{dv}{dt} = -\frac{\rho v^2}{2\beta}. \tag{5}$$

For nearly constant density over the short measured interval, the exact solution is

$$v(t) = \frac{v_0}{1 + \rho v_0 t/(2\beta)}. \tag{6}$$

We explored the deliberately broad range

$$200 \leq \beta \leq 5 \times 10^4 \ \mathrm{kg\,m^{-2}}.$$

This includes low density fragments and compact missile like bodies. An illustrative HARM-like geometry gave

$$1.42 \times 10^4 \lesssim \beta \lesssim 3.55 \times 10^4 \ \mathrm{kg\,m^{-2}},$$

when C_D was allowed to vary from 0.2 to 0.5. This is not an official missile ballistic coefficient. It is a transparent estimate based on mass, body diameter, and the assumed drag-coefficient range.

For $\beta = 10\,000\,\mathrm{kg\,m^{-2}}$, the predicted unpowered speed loss over 0.4004 s was about 6% at 500 m, 4% at 1 km, and 2% at 1.5 km. The measured sequence is too short to resolve changes of this size reliably. A lack of obvious deceleration therefore does not prove that the object was powered.

For a powered object that approximately maintains its speed, the required thrust per unit mass scales as

$$\frac{T}{m} \simeq \frac{q}{\beta}. \tag{7}$$

This shows why the low-altitude hypersonic branch remains demanding even for a dense, streamlined object: the required thrust rises with dynamic pressure and falls only for very large ballistic coefficient.

7.2 Acceleration test

We fitted the along-track motion with

$$s(t) = s_0 + v_0 t + \frac{1}{2} a_{\parallel} t^2. \tag{8}$$

We then tested the constant-velocity null hypothesis with a 10,000-trial wild bootstrap. This was not an MCMC calculation. Each trial retained the observation times and resampled the residual pattern expected from a constant-speed track.

No selected altitude showed significant acceleration or deceleration. At 500 m, the fitted value was

$$a_{\parallel} = 281.8\,\mathrm{m\,s^{-2}},$$

but the 95% null interval was

$$-1148.9\,\mathrm{m\,s^{-2}} < a_{\parallel} < +1145.9\,\mathrm{m\,s^{-2}},$$

with $p = 0.679$. At 1.5 km, the fitted value was $120.9\,\mathrm{m\,s^{-2}}$, while the null interval extended from about $-535\,\mathrm{m\,s^{-2}}$ to $+533\,\mathrm{m\,s^{-2}}$. The fitted positive values are therefore not evidence for propulsion.

We also ran 10,000 direct Monte Carlo samples at each selected altitude. These propagated the Stage 4 speed uncertainty, a small atmospheric-density uncertainty, the apparent-width uncertainty, and several reference ballistic coefficients. Target altitude was not randomly sampled because the video provides no defensible altitude prior. The intervals therefore describe uncertainty at a chosen altitude; they do not show which altitude is more likely.

7.3 Apparent-size constraint

The apparent cross track width was about 3.8 full-resolution pixels. This is an unresolved or marginally resolved width that includes the point spread function, compression, motion blur, and thermal blooming. It should be treated as an upper limit on projected cross track size rather than as a direct body dimension.

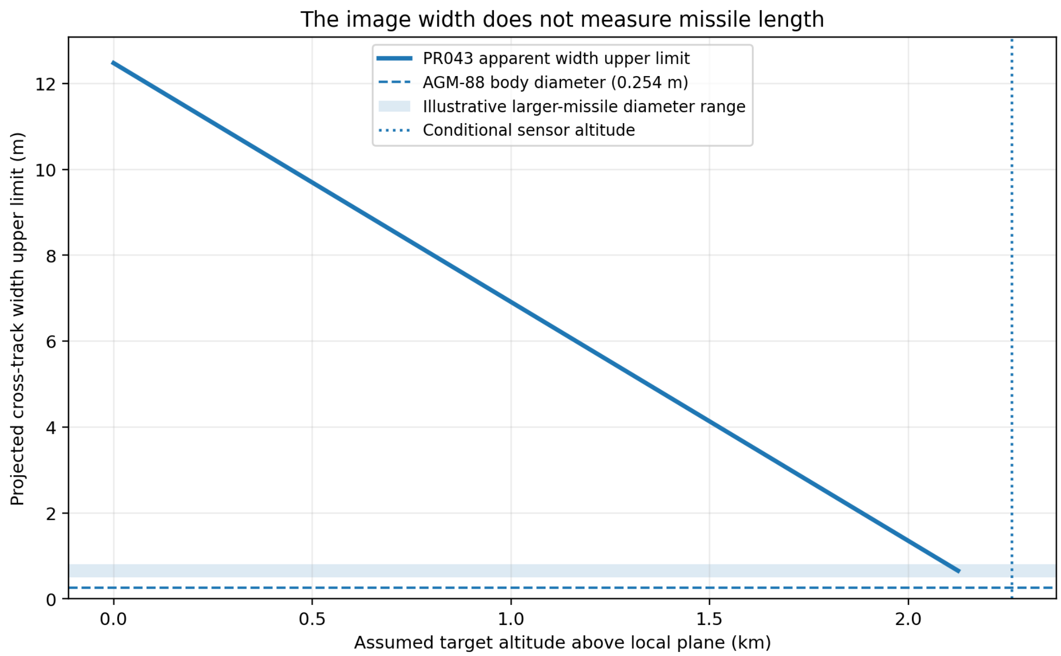

Figure 5: Altitude-dependent apparent-size constraint. The solid blue curve is the projected cross-track width upper limit inferred from the approximately 3.8-pixel image width. It decreases as the assumed target altitude approaches the sensor because the slant range decreases. The horizontal dashed line marks the published AGM-88 body diameter used only as an illustrative scale, while the pale horizontal band shows a broader missile-diameter comparison range. The vertical dotted line marks the conditional sensor altitude. None of these lines measures the target length: a long missile viewed nearly nose-on could present a cross-track dimension closer to its diameter than to its full length, and the unresolved image may be broadened by the sensor response.

The earlier value of about 4 m at 1.5 km cannot be compared directly with the published length of a missile. It is a blurred cross-track upper limit. Depending on viewing orientation, the more relevant comparison may be body diameter rather than body length.

For assumed target altitudes between approximately 0.5 km and 1.5 km, the projected cross-track upper limit is about 4–9 m. This is of the same order as the characteristic dimensions of many tactical missiles. It is therefore consistent with a missile-scale object. However, this remains an upper limit on a blurred cross-track dimension. It is not a direct measurement of the body length, and its relation to the true missile dimensions depends on viewing orientation, thermal blooming, and the sensor point-spread function.

8 Overall interpretation and limitations

The strongest result is that the released clip contains a moving image feature with a terrain-relative speed of about 801 pixels s^{-1}. The terrain match places the scene near the coordinates given above. The conditional camera model places the sensor about 2.26 km above the fitted local ground plane.

The physical target speed peculiar but not unique. If the target was near the terrain, the reconstruction gives several kilometres per second. At an assumed altitude near 2 km, the inferred speed falls to a few hundred metres per second (still supersonic). The same range uncertainty controls the apparent-size limit. This leaves two broad regimes: a more distant and exceptionally fast object, or a closer and smaller object with a lower true speed.

A fast tactical missile or a short terminal missile passage is physically compatible with part of the conditional solution family. The low-altitude hypersonic branch is strongly penalized by dynamic pressure, drag, and heating, which makes sustained cruise in that regime difficult. The short track does not show statistically significant acceleration or deceleration, so it cannot distinguish a powered missile from a sufficiently high ballistic-coefficient object that is coasting. The apparent-size estimate also does not identify a missile class. The video provides no clear plume, launch context, impact, or independent target range.

A conventional aircraft becomes more plausible only near the low-speed end of the conditional family, where the assumed target altitude approaches the conditional sensor altitude.he high-altitude end of the conditional family. A normal drone or bird is not compatible with the central distant-object solutions, but either could remain possible if the target was very close to the sensor and therefore much smaller and slower than the terrain-based reconstruction suggests. More complicated optical or infrared effects also cannot be eliminated without the original sensor metadata.

The most careful conclusion is therefore:

> The video robustly measures a small moving contrast feature at about 801 pixels s^{-1} relative to the terrain. A conditional reconstruction places the sensor about 2.26 km above the local ground plane. The inferred target speed ranges from about 3.5 km s^{-1} near the terrain to about 0.35 km s^{-1} near 2 km altitude.
>
> For assumed target altitudes of roughly 0.5–1.5 km, the inferred speed is about 1.1–2.7 km s^{-1}, while the projected cross-track upper limit is approximately 4–9 m. These values are of the same order as the speeds and characteristic dimensions of fast tactical missiles. The aerodynamic analysis further shows that a brief terminal missile passage is physically compatible with this part of the solution family.
>
> The strongest interpretation supported by the present reconstruction is therefore a fast tactical missile or terminal missile passage. However, the released clip does not determine the target range, propulsion state, or specific missile type. The unavailable sensor intrinsics and the unresolved target image prevent a unique speed, physical size, or named-system identification.